A microfluidic device for simultaneous electrical and mechanical measurements on single cells

Jian Chen,[1,2] Yi Zheng,[1,3] Qingyuan Tan,[3] Yan Liang Zhang,[3] Jason Li,[1,3]
William R. Geddie,[4] Michael A. S. Jewett,[5] and Yu Sun[1,2,3,a]

[1]*Institute of Biomaterials and Biomedical Engineering, University of Toronto,
Toronto, Ontario M5S 3G8, Canada*
[2]*Department of Electrical and Computer Engineering, University of Toronto,
Toronto, Ontario M5S 3G4, Canada*
[3]*Department of Mechanical and Industrial Engineering, University of Toronto,
Toronto, Ontario M5S 3G8, Canada*
[4]*Department of Pathology, University of Toronto, Toronto, Ontario M5G 2C4, Canada*
[5]*Department of Surgical Oncology, Princess Margaret Hospital, Toronto, Ontario
M5G 2M9, Canada*

This paper presents a microfluidic device for simultaneous mechanical and electrical characterization of single cells. The device performs two types of cellular characterization (impedance spectroscopy and micropipette aspiration) on a single chip to enable cell electrical and mechanical characterization. To investigate the performance of the device design, electrical and mechanical properties of MC-3T3 osteoblast cells were measured. Based on electrical models, membrane capacitance of MC-3T3 cells was determined to be 3.39 ± 1.23 and 2.99 ± 0.82 pF at the aspiration pressure of 50 and 100 Pa, respectively. Cytoplasm resistance values were 110.1 ± 37.7 kΩ (50 Pa) and 145.2 ± 44.3 kΩ (100 Pa). Aspiration length of cells was found to be 0.813 ± 0.351 μm at 50 Pa and 1.771 ± 0.623 μm at 100 Pa. Quantified Young's modulus values were 377 ± 189 Pa at 50 Pa and 344 ± 156 Pa at 100 Pa. Experimental results demonstrate the device's capability for characterizing both electrical and mechanical properties of single cells. © *2011 American Institute of Physics.* [doi:10.1063/1.3571530]

I. INTRODUCTION

The electrical properties of the cell membrane and cytoplasm[1–3] and the mechanical properties of the cytoskeleton[4,5] determine the overall biophysical properties of a cell. The electrical and/or mechanical characterization of single cells is fundamental for understanding cell properties and has also been correlated with pathophysiological states in diseases, such as malaria[6–12] and cancer.[13–20]

Advances in microfluidic technologies have led to the development of microdevices for single-cell electrical property characterization. The three types of microdevices for electrical characterization are based on patch clamp,[21–34] electrorotation,[35–40] and micro-electrical impedance spectroscopy (μ-EIS).[1–3] Patch-clamp microdevices characterize cellular ion channel activities by sucking a cell membrane patch into a micropipette to form a high electrical resistance seal. This technique is invasive since the cell membrane is intentionally disrupted, and thus cannot be used for long-term study or multiple types of measurements. In electrorotation, a rotating electric field is exerted on a suspended cell causing the cell to rotate as a result of Maxwell–Wanger polariza-

---

[a]Author to whom correspondence should be addressed. Electronic mail: sun@mie.utoronto.ca. Tel.: 1-416-946-0549. FAX: 1-416-978-7753.

5, 014113-1   © 2011 American Institute of Physics

tion. Electrorotation is a powerful technique for measuring cell membrane permittivity and cytoplasm conductivity. However, accurate cell positioning in the rotating electrical field is required, making the implementation of this technique labor intensive.

μ-EIS is a noninvasive technique in which a frequency-dependent excitation signal is applied across a single cell to measure the corresponding current response.[1–3] Several microfluidic devices have recently been reported for single-cell impedance measurement using coplanar[41,42] and parallel[43–47] facing electrodes. Hydrodynamic trapping methods have been employed in conjunction with μ-EIS for measuring cellular impedance properties over extended periods of time.[11,48–50] Furthermore, two mechanisms utilizing vacuum aspiration[13,14] and electrode surface modification[51] were proposed to form tight cell adhesion on the measurement electrodes. In addition, microhole-based chips modified from patch-clamp devices have been proposed to address the leakage current issue by forming proper sealing between the aspirated cell and the aspiration channel.[52,53] The main concern of the μ-EIS technique is that differences in impedance profiles between measurements taken with and without a cell's presence are usually small and sometimes unobservable.[51]

In the meantime, several microfluidic-based devices have also been developed to measure the mechanical properties of single cells, such as micropipette aspiration,[54,55] electrodeformation,[56–58] and optical stretchers.[16,20,59,60] In micropipette aspiration, a cell is deformed by applying negative pressure through an aspiration channel. By recording the resulting geometrical changes of the cell and using well-established aspiration mechanics models, raw data can be used to extract the cell's Young's modulus. In electrodeformation, a cell placed in an applied electric field becomes polarized due to the build-up of surface charges and therefore is deformed electrically. By interpreting the relationship between the deformation ratio and the applied electric field, cell mechanical properties can be obtained. In an optical stretcher, a two-beam laser trap is optimized to serially deform single suspended cells by optically induced surface forces to measure mechanical properties.

Discussions above reveal that a number of microfluidic devices have been demonstrated for cell biophysical characterization. However, the majority of these devices are only capable of characterizing either electrical properties (i.e., ion channel activities, membrane capacitance, and cytoplasm resistance) or mechanical properties (i.e., Young's modulus) of a cell. For a more complete understanding of a cell's properties, it is desirable to perform both electrical and mechanical measurements on the same cell using the same device. The only device, which was reported to perform both impedance and mechanical characterization of single cells,[11] is complex in both design and microfabrication processes. In this device, cantilever deformation ratios were used to indicate cell mechanical properties, which are difficult to be translated into cell's Young's modulus. The design electrically suffered from the problem of leakage currents, and no electrical model is available for the interpretation of the raw data into cell's electrical parameters. In terms of microfabrication, four photolithography steps, dry and wet etching of silicon, and metal and dielectric deposition and lift-off were required for device construction.

This study presents a microfluidic device for single-cell electrical and mechanical characterization using impedance spectroscopy and micropipette aspiration (see Fig. 1). The device, consisting of two layers of Polydimethylsiloxane (PDMS), is simple in both design and fabrication. The application of a low negative pressure traps a single cell at the entrance of the aspiration channel while the magnitude of this pressure controls the cell aspiration length. Cellular deformation is recorded as a function of increasing pressure while cellular impedance is measured via two Ag/AgCl electrodes inserted into culture medium. The design of this device overcomes several technological limitations: (1) the leakage current is minimized through proper sealing between the aspirated cell and the aspiration channel; (2) the electrode polarization problem (impedance profile distortion in the low frequency domain due to the effect of the electrical double layer) is minimized by using Ag/AgCl nonpolarizable electrodes;[61] (3) equivalent circuit models are straightforward to establish for determining cellular components (e.g., membrane capacitance and cytoplasm resistance); and (4) existing micropipette aspiration models enable the quantitative extraction of the Young's modulus values of cells.
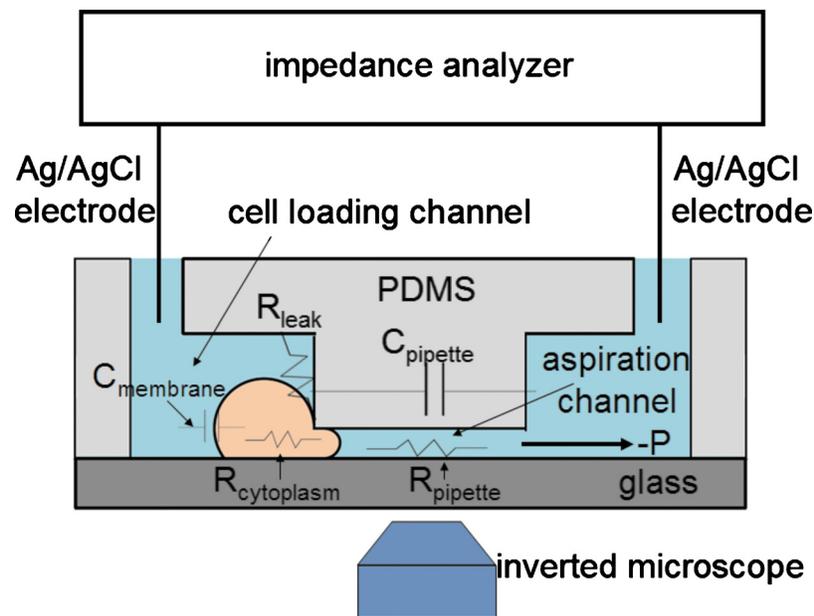
FIG. 1. Simultaneous electrical and mechanical characterization of single cells. A negative pressure is applied to trap a single cell at the entrance of the aspiration channel. Cell deformations are recorded by imaging. Impedance measurement is conducted via two Ag/AgCl electrodes connected with an impedance analyzer. The electrical model of the aspiration channel is represented by $R_{pipette}$ and $C_{pipette}$ in parallel. Cellular electrical components are represented by $R_{cytoplasm}$ and $C_{membrane}$ in series. R_{leak} indicates sealing during cell aspiration.

II. MATERIALS AND METHODS

A. Materials

Unless otherwise indicated, all chemicals were obtained from Sigma-Aldrich (Oakville, ON, Canada) and cell-culture reagents were from American Type Culture Collection (ATCC) (Manassas, VA, USA). Materials required for device fabrication included SU-8 photoresist (MicroChem Corp., Newton, MA, USA) and 184 silicone elastomer (Ellsworth Adhesives Canada, Burlington, ON, Canada).

B. Device fabrication

1. SU-8 mold master fabrication

The two-layer channel masters (see Fig. 2) were fabricated in the clean room facility of the Emerging Communications Technology Institute (ECTI) at the University of Toronto. Glass slides were cleaned in acetone, methanol, and de-ionized water, and dried on a hot plate
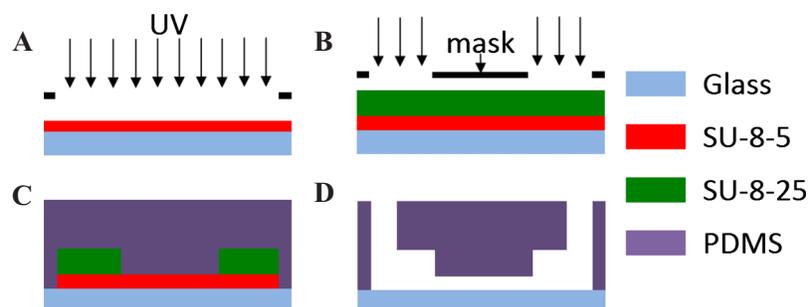

FIG. 2. Fabrication steps for forming the two-layer PDMS device.

(30 min @ 150 °C). The first layer of SU-8 (5 μm thick) is made of SU-8-5 to form cell aspiration channels, which was spun on the slide (500 rpm for 5 s+1500 rpm for 30 s), soft-baked (2 min @ 65 °C+5 min @ 95 °C), and exposed to UV light (7 s, 16 mW cm^2, 365 nm) through the first chrome-on-glass mask (University of Alberta Nanofabrication Facility, Edmonton, Alberta, Canada) using a Karl Suss MA6 mask aligner (Garching, Germany). Slides were then baked on a hot plate (1 min @ 65 °C+2 min @ 95 °C) to cross-link the exposed SU-8-5 without development [Fig. 2(a)].

The second layer of SU-8 (25 μm thick) is made of SU-8-25 to form cell loading channels. SU-8-25 was spin coated on the glass slide covered with the first layer of SU-8-5 (without development) (500 rpm for 5 s+2000 rpm for 30 s), soft-baked (3 min @ 65 °C +7 min @ 95 °C), aligned, and exposed to UV light (12 s, 16 mW cm^2, 365 nm) through the second chrome-on-glass mask (University of Alberta Nanofabrication Facility, Edmonton, Alberta, Canada) [see Fig. 2(b)]. Slides were then baked on a hot plate (1 min @ 65 °C +3 min @ 95 °C) to cross-link the exposed SU-8-25, developed in SU-8 developer for 60 s, and finally hard baked (2 h @ 175 °C).

2. PDMS molding and channel bonding

PDMS prepolymer and curing agent were mixed at a ratio of 10:1, degassed in a vacuum desiccator, poured on a channel master placed in an aluminum foil plate, and finally baked in a convection oven (15 min @ 125 °C) [see Fig. 2(c)]. PDMS channels were then peeled from the SU-8 master and reservoir holes were punched through. Bonding to glass slides was conducted using a portable corona treater where PDMS pieces and glass slides were treated with a BD20-AC corona treater (Electro-Technic Products, Inc., Chicago, IL, USA) for 30 s per piece, pressed together, and baked on a hot plate (1 h @ 100 °C) [see Fig. 2(d)].

C. Device operation

MC-3T3 cells were purchased from American Type Culture Collection (Manassas, VA, USA) and cultured in GIBCO™ Minimum Essential Medium Alpha (1X) supplemented with 10% fetal bovine serum. Cells were cultured in tissue culture-treated polystyrene flasks. Immediately prior to an experiment, cells were trypsinized, centrifuged, and resuspended in GIBCO™ Minimum Essential Medium Alpha (1X) with a concentration of 1×10^6 cells/ml. Cell passage generations between p3 and p10 were used in this experiment.

The device was first filled with culture medium. Before cell trapping, an impedance profile was recorded for reference (Agilent-4294A Impedance Analyzer, Agilent Technologies, Inc., Santa Clara, CA, USA). A droplet of cell suspension (MC-3T3 cells) was then pipetted to the entrance of the cell loading channel. A negative pressure from 50 to 100 Pa generated from a custom developed pump was applied to trap and aspirate a cell at the entrance of the cell aspiration channel. Cell images were taken by an inverted microscope (Olympus IX801, Olympus Canada, Inc., Markham, ON, Canada). Impedance data with the frequency range of 100 Hz–1 MHz (excitation voltage: 100 mV) were recorded by the impedance analyzer. After characterization, a high negative pressure ($\sim$2000 Pa) was used to completely remove the cell from the aspiration channel. Thus, the device was ready to perform measurements on the next cell.

D. Data analysis

1. Impedance profile analysis

To interpret the measured impedance data, three electrical models are proposed (see Fig. 3), which were modified from equivalent electrical models used in the patch-clamp technique.[27] Model 1 is used to fit the impedance data without cell trapping, in which $R_{pipette}$ and $C_{pipette}$ represent the equivalent resistance and capacitance of the aspiration channel (see Fig. 1). Models 2 and 3 are used to model the situation with cell trapping. R_{leak} in model 2 represents the cell blockage of electrical filed (see Fig. 1), and this model does not include cell's electrical components. In model 3, cellular electrical components are considered, which are represented as
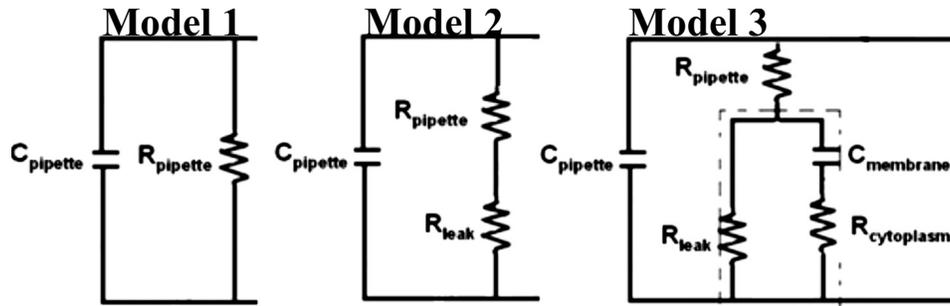
FIG. 3. Circuit models proposed to assess impedance data. Model 1 is used to interpret impedance profiles with no cell trapping, aiming to calculate the values of $R_{pipette}$ and $C_{pipette}$ for their further use in models 2 and 3. Models 2 and 3 are used to model the situations with cell trapping. In model 2, cellular electrical components are not considered and R_{leak} is used to represent cell blockage of electrical filed. In model 3, cellular electrical components are taken into consideration in which the cell membrane is represented by a capacitor $C_{membrane}$ and the cell cytoplasm is represented by a resistor $R_{cytoplasm}$.

$C_{membrane}$ (capacitance of the cell membrane) and $R_{cytoplasm}$ (resistance of the cytoplasm) connected in series. In these equivalent circuit models, the electrical double layer issue was not considered since Ag/AgCl nonpolarizable electrodes were used, and therefore no electrical double layer was produced.[61]

MATLAB programs (MathWork, Natick, MA, USA) were developed to fit the impedance profiles to the aforementioned electrical models. Since the mathematic expressions of these models are highly nonlinear, nonlinear least-squares fitting was employed for optimization.[62] In order to address the potential concern of convergence to a local solution due to the inappropriate choice of a group of initial values, a loop function was used to enumerate the initial values of interest, subsequent to which nonlinear least-squares curve fitting was conducted for each case. Optimization results from each group of initial values were then compared to locate the best curve fitting case and the corresponding optimized parameters.

2. Image processing of cell aspiration and Young's modulus calculation

In order to quantify the aspiration length, a subpixel contour extraction algorithm was developed to process the captured images. The procedure consists of a sequence of image processing steps adapted to the context of cell elongation (such as smoothing, thresholding, edge detection, followed by a Hough transform). The Young's modulus values of the aspirated cells were calculated according to $E = (3\Phi/2\pi)\Delta P(R/L)$, based on the elastic half-space solid model,[63,64] where E is the Young's modulus of the cell, ΔP is the applied negative pressure, R is the inner radius of the microchannel, and Φ is a constant with a typical value set at 2.1.

III. RESULTS AND DISCUSSION

Differences in impedance profiles between measurements with and without single cells are usually small and sometimes unobservable.[51] For example, the differential single-cell impedance analysis using hydrodynamic cell trapping, reported in Ref. 48, had only a 20%–30% impedance difference with and without cell trapping. This small difference can be due to poor contact between the cell and electrodes, which led to current leakage.[14]

To improve cell-electrode adhesion, a μ-EIS was developed where a negative pressure was used to suck the measured cell into close contact with the electrodes.[14] Differences were observed in impedance phase profiles of two cell lines. However, the impedance amplitude was not found statistically different, which proves the existence of leakage current although tight cell-electrode adhesion was formed. Another approach to reduce leakage current involves surface modification of the electrode and minimization of microelectrode contact with the electrolyte,[51] which resulted in an impedance amplitude increase of approximately 40% in the low frequency domain (several

kilohertz). However, at these frequencies the amplitude difference is dominated by the presence of an electric double layer suggesting that the observed increase in impedance amplitude may result from the disturbance of the electrical double layer (versus from the cell). It was speculated in Ref. 51 that the nanometer gap between a cell and electrodes is the current leakage source and the effect of the electrical double layer due to electrode polarization can further distort impedance profiles in the low frequency domain.

In order to further reduce the leakage current and remove the electrical double layer effect, a microhole-based chip modified from the vertical patch-clamp technique utilizing the four-electrode arrangement was proposed.[52] This approach resulted in a greater than 100% impedance amplitude increase after cell trapping. It can be further improved by proper control of the aspiration pressure to form a tight seal between the cell and the microhole, mimicking the situation used in conventional patch-clamping (i.e., gigaohm seal).

The microfluidic device developed in this study is based on lateral patch-clamping and micropipette aspiration. Compared to the microhole-based device,[52] this design has a few advantages: (1) accurate control of negative pressure enables a proper seal of the cell with the aspiration channel to minimize the leakage current issue; (2) the device performs lateral aspiration rather than vertical aspiration (as in Ref. 52), enabling microscopy measurement of cell elongation, and thus mechanical characterization while electrical impedance profiles are measured; and (3) the geometry of lateral aspiration dramatically reduces the capacitive coupling between the cell loading channel and the aspiration channel, which is important for low-noise impedance recording.

A. Impedance measurement results and data analysis

Figure 4 shows the impedance amplitude profiles [Fig. 4(a)] and phase profiles [Fig. 4(b)] as a function of frequency, both with and without cell trapping at an aspiration pressure of 50 and 100 Pa, respectively. Error bars represent standard deviations (n=18). The values of measured impedance amplitude and phase at "no cell trapping" are steady in the low and medium frequency domains (433.7 ± 50.1 kΩ and $-0.1 \pm 0.015°$ at 1 kHz), modeled as a pure resistor $R_{pipette}$. The average values are consistent with those reported by Cho *et al.*[52] Since Ag/AgCl electrodes were used in this design, the electrical double layer effect was not observed. In the high frequency domain, a decrease in both amplitude and phase occurred (374.7 ± 35.5 kΩ and $-25.5 \pm 4.8°$ at 1 MHz), indicating the presence of a capacitance, $C_{pipette}$.

Circuit model 1 was used to fit the impedance profiles at no cell trapping. The calculated $R_{pipette}$ and $C_{pipette}$ are 434.4 ± 50.3 kΩ and 0.19 ± 0.03 pF. The transition frequency at which impedance amplitude starts to decrease is roughly 100 kHz, which is much higher than the transition frequency (~ 5 kHz) in Cho *et al.*,[52] indicating a lower parasitic capacitance $C_{pipette}$ present in this design because of the lateral aspiration structure.[22,32]

The values of measured impedance amplitude and phase at "cell trapping at 50 Pa" are also steady in the low and medium frequency domains (601.9 ± 54.6 kΩ and $-0.19 \pm 0.055°$ at 1 kHz) [see Figs. 5(a) and 5(b)], modeled as two resistors ($R_{pipette}$ and $R_{leak(50\ Pa)}$) connected in series. R_{leak} indicates cell blockage of the electrical field at the entrance of the aspiration channel. In the high frequency domain, a decrease in both amplitude and phase occurred (414.5 ± 31.3 kΩ and $-31.5 \pm 3.4°$ at 1 MHz).

Circuit models 2 and 3 were used to fit the impedance profiles at cell trapping at 50 Pa. Compared to model 2, model 3 better fits the impedance data [see Figs. 5(a) and 5(b)], proving that the data reflect the properties of the cells. The values $R_{leak(50\ Pa)}$, $C_{membrane}$, and $R_{cytoplasm}$ using model 3 were determined to be 167.5 ± 46.7 kΩ, 3.39 ± 1.23 pF, and 110.1 ± 37.7 kΩ (see Fig. 6).

Compared to the patch-clamp technique, R_{leak} obtained here is relatively low. Since the aspiration channel in this device is not exactly circular, forming effective seal between the cell membrane and the aspiration channel is more difficult and leakage may have taken place.[65] The calculated $C_{membrane}$ values are consistent with those (roughly 1 μF/cm^2) obtained from patch clamp.[66]
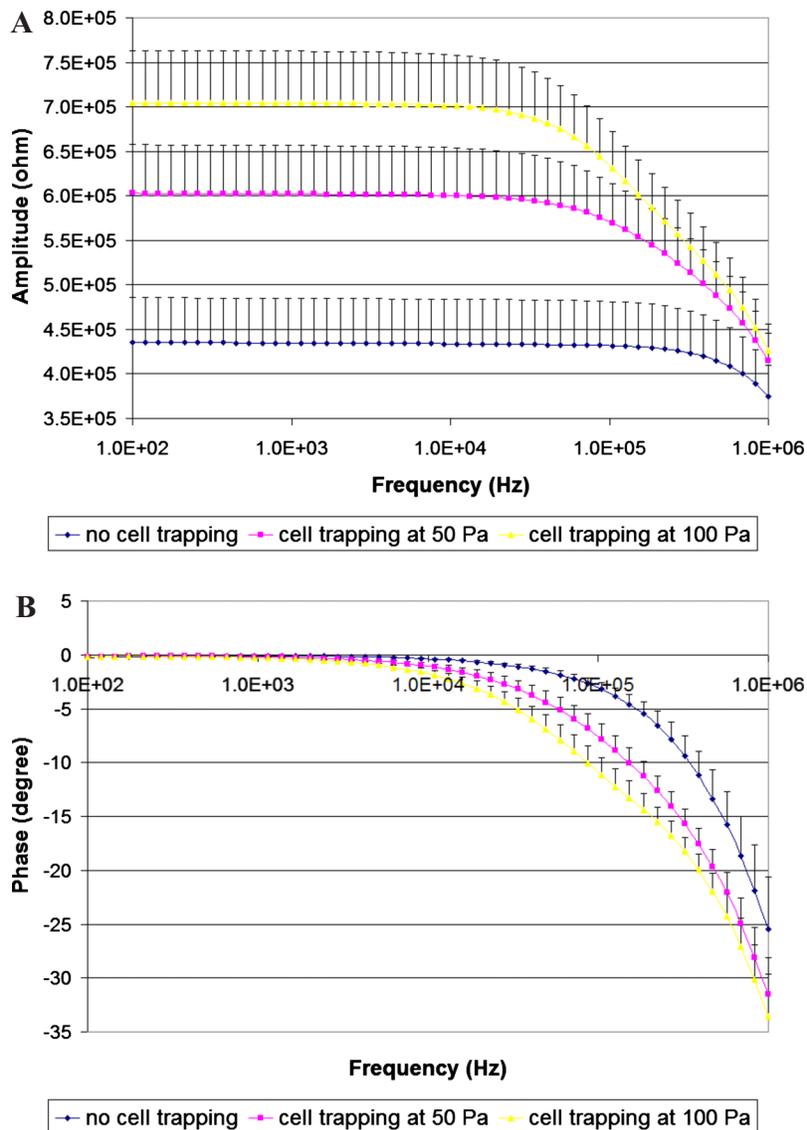
FIG. 4. Measured impedance amplitude (a) and phase (b) at no cell trapping, cell trapping at 50 Pa, and cell trapping at 100 Pa as a function of frequency (n=18). Error bars represent standard deviation.

The values of measured impedance amplitude and phase at cell trapping at 100 Pa are steady in the low and medium frequency domains (704.2 ± 58.3 kΩ and $-0.30 \pm 0.007°$ at 1 kHz) [see Figs. 5(c) and 5(d)], modeled as two resistors ($R_{pipette}$ and $R_{leak(100\ Pa)}$) in series. In the high frequency domain, a decrease in both amplitude and phase occurred (426.6 ± 29.8 kΩ and $-33.5 \pm 3.9°$ at 1 MHz).

Circuit models 2 and 3 were used to fit the impedance profiles at "cell trapping at 100 Pa." Similar to the case cell trapping at 50 Pa, model 3 better fits the impedance data [see Figs. 5(c) and 5(d)], demonstrating that the data reflect cell properties. $R_{leak(100\ Pa)}$, $C_{membrane}$, and $R_{cytoplasm}$ using model 3 were determined to be 272.5 ± 57.0 kΩ, 2.99 ± 0.82 pF, and 145.2 ± 44.3 kΩ (see Fig. 6). $R_{leak(100\ Pa)}$ is 60% higher than $R_{leak(50\ Pa)}$, which indicates a better seal of the cell with the aspiration channel at 100 Pa, and therefore a further decrease in leakage current. As the aspiration pressure was increased from 50 to 100 Pa, a larger portion of a cell was aspirated into the aspiration channel, which causes a roughly 30% increase in $R_{cytoplasm}$.
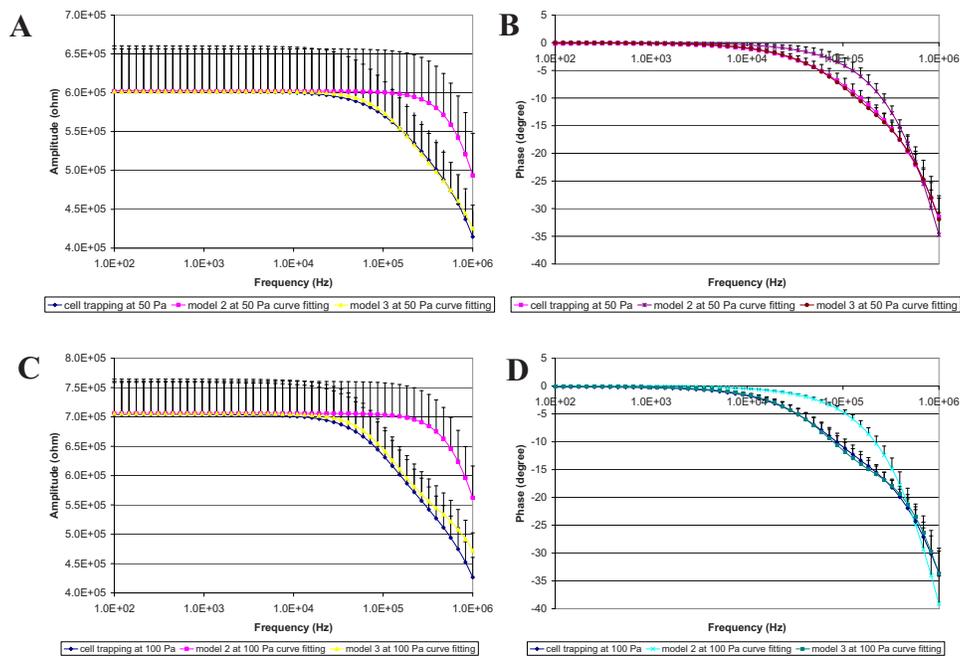
FIG. 5. Fitting measured impedance data with cell trapping to electrical models 2 and 3. (a) Fitting measurement impedance amplitude profiles at cell trapping at 50 Pa to models 2 and 3. (b) Fitting measurement impedance phase profiles at cell trapping at 50 Pa to models 2 and 3. (c) Fitting measurement impedance amplitude profiles at cell trapping at 100 Pa to models 2 and 3. (d) Fitting measurement impedance phase profiles at cell trapping at 100 Pa to models 2 and 3. Compared to model 2, model 3 better fits the impedance data (both amplitude and phase), demonstrating that the measurement results reflect cell properties. Error bars represent standard deviation.

As to the 10% $C_{membrane}$ decrease, it is also possibly caused by cell shape change. $C_{membrane}$ is represented by two capacitors in series. The first capacitor corresponds to the portion of the membrane sucked into the aspiration channel, and the second capacitor corresponds to the portion of the membrane outside the aspiration channel. When the aspiration pressure increases, there is no change for the effective area of the portion of the membrane sucked into the aspiration, which is determined by the cross-section of the channel. At the same time, the effective area of the cell membrane outside the channel decreases, causing $C_{membrane}$ to decrease.

It is worth noting that in the impedance characterization microdevices using vacuum aspiration for cell positioning, there is a potential concern that aspiration pressures may modulate the on-off stages of mechanical-sensitive ion channels on cell membranes, and therefore affect impedance profiles. In this study, this concern was not taken into consideration as in existing literature.[13,14,52,53] The reason is that the lowest current measured in our experiments was several μAs (excitation voltage: 100 mV, the highest impedance amplitude collected <800 kΩ), which is three orders higher than the typical current level in ion channel experiments (several nAs only),[23,27,29,33] proving that the effect of ion channels is negligible.

B. Cell aspiration results and Young's modulus calculation

Figure 7(a) shows the morphology of a cell before aspiration and at a negative pressure of 100 Pa. Aspiration length of cells (n=18) was found to be 0.813 ± 0.351 μm at 50 Pa and 1.771 ± 0.623 μm at 100 Pa [see Fig. 7(b)]. Calculated Young's modulus values of MC-3T3 cells were 377 ± 189 Pa at 50 Pa and 344 ± 156 Pa at 100 Pa using the infinite half-space model of conventional micropipette aspiration.[64]

Since the aspiration channel in this device is not exactly circular, forming a perfect seal between the cell and the aspiration channel is difficult and leakage may take place at the corners of the aspiration channel. This leakage may result in higher vacuum pressure required to aspirate
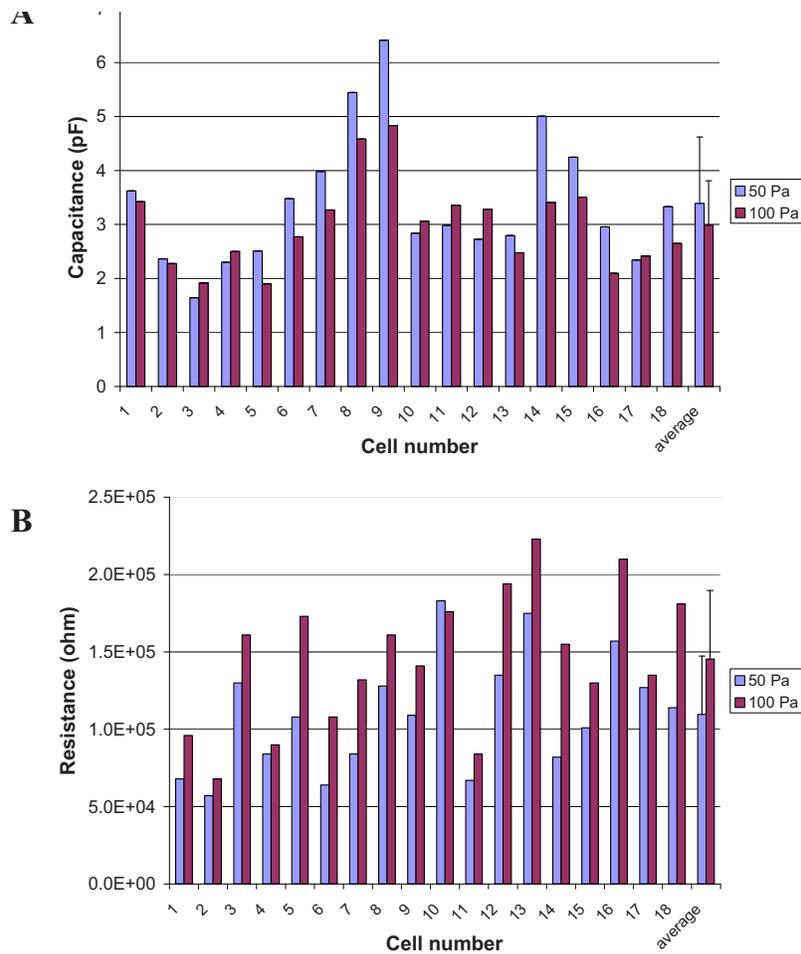
FIG. 6. Calculated cell membrane capacitance (a) and cytoplasm resistance (b) of MC-3T3 cells (n=18) by fitting the experimental results with model 3 under aspiration pressure of 50 and 100 Pa, respectively. The average values and standard deviations of membrane capacitance and cytoplasm resistance were also shown in the last columns of the figure.

cells to a certain distance compared to conventional micropipettes, possibly resulting in Young's modulus values lower than the use of conventional glass micropipettes. Interestingly, the Young's modulus values of 377 ± 189 Pa at 50 Pa and 344 ± 156 Pa at 100 Pa determined using this microdevice are not much lower than those obtained from the use of conventional micropipettes on the same type of cells (555 ± 183 Pa).[67] The insignificant difference can be attributed to the fact that the 5 μm microchannels exhibit a vaulted rather than a strictly rectangular cross-section, alleviating the leakage problem to an extent compared to perfect rectangular aspiration channels.[23,33]

IV. CONCLUSION

This paper demonstrated the use of a microdevice for both electrical and mechanical characterization of single cells using impedance spectroscopy and micropipette aspiration on the same device. Impedance profiles and cell aspiration lengths were recorded by an impedance analyzer and microscopy imaging. Membrane capacitance of MC-3T3 cells was found to be 3.39 ± 1.23 and 2.99 ± 0.82 pF at the aspiration pressure of 50 and 100 Pa, respectively, while cytoplasm resistance values were determined to be 110.1 ± 37.7 kΩ (50 Pa) and 145.2 ± 44.3 kΩ (100 Pa). Quantified Young's modulus was 377 ± 189 Pa at 50 Pa and 344 ± 156 Pa at 100 Pa.
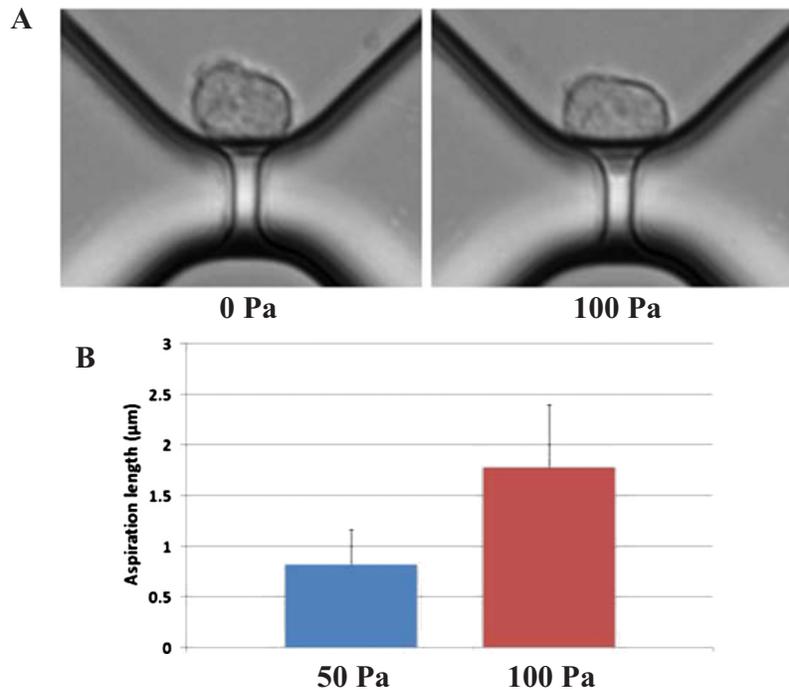
FIG. 7. (a) Images of cell aspiration at 0 and 100 Pa. (b) Aspiration lengths of cells at 50 Pa (0.813 ± 0.351 μm) and 100 Pa (1.771 ± 0.623 μm) (n=18). Calculated Young's modulus values are 377 ± 189 Pa at 50 Pa and 344 ± 156 Pa at 100 Pa. Error bars represent standard deviation.

[1] H. Morgan, T. Sun, D. Holmes, S. Gawad, and N. G. Green, J. Phys. D **40**, 61 (2007).
[2] T. Sun and H. Morgan, Microfluid. Nanofluid. **8**, 423 (2010).
[3] A. Valero, T. Braschler, and P. Renaud, Lab Chip **10**, 2216 (2010).
[4] D. H. Boal, *Mechanics of the Cell* (Cambridge University Press, Cambridge, 2002).
[5] C. R. Ethier and C. A. Simmons, *Introductory Biomechanics: From Cells to Organisms* (Cambridge University Press, Cambridge, 2007).
[6] F. K. Glenister, R. L. Coppel, A. F. Cowman, N. Mohandas, and B. M. Cooke, Blood **99**, 1060 (2002).
[7] J. P. Mills, L. Qie, M. Dao, C. T. Lim, and S. Suresh, Mech. Chem. Biosyst. **1**, 169 (2004).
[8] G. B. Nash, E. O'Brien, E. C. Gordon-Smith, and J. A. Dormandy, Blood **74**, 855 (1989).
[9] M. Paulitschke and G. B. Nash, J. Lab. Clin. Med. **122**, 581 (1993).
[10] S. Suresh, J. Spatz, J. P. Mills, A. Micoulet, M. Dao, C. T. Lim, M. Beil, and T. Seufferlein, Acta Biomater. **1**, 15 (2005).
[11] Y. H. Cho, T. Yamamoto, Y. Sakai, T. Fujii, and B. Kim, J. Microelectromech. Syst. **15**, 287 (2006).
[12] J. E. Gordon, Z. Gagnon, and H. C. Chang, Biomicrofluidics **1**, 044102 (2007).
[13] K. H. Han, A. Han, and A. B. Frazier, Biosens. Bioelectron. **21**, 1907 (2006).
[14] Y. Cho, H. S. Kim, A. B. Frazier, Z. G. Chen, D. M. Shin, and A. Han, J. Microelectromech. Syst. **18**, 808 (2009).
[15] S. E. Cross, Y. S. Jin, J. Rao, and J. K. Gimzewski, Nat. Nanotechnol. **2**, 780 (2007).
[16] J. Guck, S. Schinkinger, B. Lincoln, F. Wottawah, S. Ebert, M. Romeyke, D. Lenz, H. M. Erickson, R. Ananthakrishnan, D. Mitchell, J. Kas, S. Ulvick, and C. Bilby, Biophys. J. **88**, 3689 (2005).
[17] M. Lekka, P. Laidler, D. Gil, J. Lekki, Z. Stachura, and A. Z. Hrynkiewicz, Eur. Biophys. J. **28**, 312 (1999).
[18] M. Makale, Birth Defects Res. C **81**, 329 (2007).
[19] K. A. Ward, W. I. Li, S. Zimmer, and T. Davis, Biorheology **28**, 301 (1991).
[20] F. Wottawah, S. Schinkinger, B. Lincoln, S. Ebert, K. Muller, F. Sauer, K. Travis, and J. Guck, Acta Biomater. **1**, 263 (2005).
[21] C. C. Chen and A. Folch, Lab Chip **6**, 1338 (2006).
[22] N. Fertig, R. H. Blick, and J. C. Behrends, Biophys. J. **82**, 3056 (2002).

[23] C. Ionescu-Zanetti, R. M. Shaw, J. G. Seo, Y. N. Jan, L. Y. Jan, and L. P. Lee, Proc. Natl. Acad. Sci. U.S.A. **102**, 9112 (2005).
[24] K. G. Klemic, J. F. Klemic, M. A. Reed, and F. J. Sigworth, Biosens. Bioelectron. **17**, 597 (2002).
[25] T. Lehnert, M. A. M. Gijs, R. Netzer, and U. Bischoff, Appl. Phys. Lett. **81**, 5063 (2002).
[26] T. Lehnert, D. M. T. Nguyen, L. Baldi, and M. A. M. Gijs, Microfluid. Nanofluid. **3**, 109 (2007).
[27] S. Li and L. W. Lin, Sens. Actuators, A **134**, 20 (2007).
[28] B. Matthews and J. W. Judy, J. Microelectromech. Syst. **15**, 214 (2006).
[29] W. L. Ong, J. S. Kee, A. Ajay, N. Ranganathan, K. C. Tang, and L. Yobas, Appl. Phys. Lett. **89**, 093902 (2006).
[30] W. L. Ong, K. C. Tang, A. Agarwal, R. Nagarajan, L. W. Luo, and L. Yobas, Lab Chip **7**, 1357 (2007).
[31] S. Pandey, R. Mehrotra, S. Wykosky, and M. H. White, Solid-State Electron. **48**, 2061 (2004).
[32] R. Pantoja, J. M. Nagarah, D. M. Starace, N. A. Melosh, R. Blunck, F. Bezanilla, and J. R. Heath, Biosens. Bioelectron. **20**, 509 (2004).
[33] J. Seo, C. Ionescu-Zanetti, J. Diamond, R. Lal, and L. P. Lee, Appl. Phys. Lett. **84**, 1973 (2004).
[34] A. Stett, V. Bucher, C. Burkhardt, U. Weber, and W. Nisch, Med. Biol. Eng. Comput. **41**, 233 (2003).
[35] C. Dalton, A. D. Goater, J. P. H. Burt, and H. V. Smith, J. Appl. Microbiol. **96**, 24 (2004).
[36] G. De Gasperis, X. B. Wang, J. Yang, F. F. Becker, and P. R. C. Gascoyne, Meas. Sci. Technol. **9**, 518 (1998).
[37] R. Holzel, Biochimica Et Biophysica Acta-Molecular Cell Research **1450**, 53 (1999).
[38] M. Kriegmaier, M. Zimmermann, K. Wolf, U. Zimmermann, and V. L. Sukhorukov, Biochimica Et Biophysica Acta-General Subjects **1568**, 135 (2001).
[39] J. Yang, Y. Huang, X. Wang, X. B. Wang, F. F. Becker, and P. R. C. Gascoyne, Biophys. J. **76**, 3307 (1999).
[40] X. F. Zhou, J. P. H. Burt, and R. Pethig, Phys. Med. Biol. **43**, 1075 (1998).
[41] S. Gawad, L. Schild, and P. Renaud, Lab Chip **1**, 76 (2001).
[42] L. L. Sohn, O. A. Saleh, G. R. Facer, A. J. Beavis, R. S. Allan, and D. A. Notterman, Proc. Natl. Acad. Sci. U.S.A. **97**, 10687 (2000).
[43] K. Cheung, S. Gawad, and P. Renaud, Cytometry, Part A **65A**, 124 (2005).
[44] S. Gawad, K. Cheung, U. Seger, A. Bertsch, and P. Renaud, Lab Chip **4**, 241 (2004).
[45] D. Holmes and H. Morgan, Anal. Chem. **82**, 1455 (2010).
[46] D. Holmes, D. Pettigrew, C. H. Reccius, J. D. Gwyer, C. van Berkel, J. Holloway, D. E. Davies, and H. Morgan, Lab Chip **9**, 2881 (2009).
[47] D. Holmes, J. K. She, P. L. Roach, and H. Morgan, Lab Chip **7**, 1048 (2007).
[48] S. Z. Hua and T. Pennell, Lab Chip **9**, 251 (2009).
[49] L. S. Jang and M. H. Wang, Biomed. Microdevices **9**, 737 (2007).
[50] D. Malleo, J. T. Nevill, L. P. Lee, and H. Morgan, Microfluid. Nanofluid. **9**, 191 (2010).
[51] M. Thein, F. Asphahani, A. Cheng, R. Buckmaster, M. Q. Zhang, and J. Xu, Biosens. Bioelectron. **25**, 1963 (2010).
[52] S. B. Cho and H. Thielecke, Biosens. Bioelectron. **22**, 1764 (2007).
[53] C. D. James, N. Reuel, E. S. Lee, R. V. Davalos, S. S. Mani, A. Carroll-Portillo, R. Rebeil, A. Martino, and C. A. Apblett, Biosens. Bioelectron. **23**, 845 (2008).
[54] W. Kim and A. Han, The 14th International Conference on Miniaturized Systems for Chemistry and Life Sciences (μTAS 2010), Groningen, The Netherlands, 2010, pp. 253–255.
[55] C. Moraes, J. H. Tong, X. Y. Liu, C. A. Simmons, and Y. Sun, The 11th International Conference on Miniaturized Systems for Chemistry and Life Sciences (μTAS 2007), Paris, France, 2007, pp. 751–753.
[56] L. A. MacQueen, M. D. Buschmann, and M. R. Wertheimer, J. Micromech. Microeng. **20**, 065007 (2010).
[57] P. K. Wong, W. Tan, and C. M. Ho, J. Biomech. **38**, 529 (2005).
[58] U. Zimmermann, U. Friedrich, H. Mussauer, P. Gessner, K. Hamel, and V. Sukhorukov, IEEE Trans. Plasma Sci. **28**, 72 (2000).
[59] J. Guck, R. Ananthakrishnan, H. Mahmood, T. J. Moon, C. C. Cunningham, and J. Kas, Biophys. J. **81**, 767 (2001).
[60] J. Guck, R. Ananthakrishnan, T. J. Moon, C. C. Cunningham, and J. Kas, Phys. Rev. Lett. **84**, 5451 (2000).
[61] W. Feder, J. Appl. Physiol. **18**, 397 (1963).
[62] T. F. Coleman and Y. Y. Li, SIAM J. Optim. **6**, 418 (1996).
[63] E. A. Evans and P. L. La Celle, Blood **45**, 29 (1975).
[64] R. M. Hochmuth, J. Biomech. **33**, 15 (2000).
[65] M. Abdelgawad, C. Wu, W.-Y. Chien, W. R. Geddie, M. A. S. Jewett, and Y. Sun, Lab Chip **11**, 545 (2011).
[66] H. Zhang, A. L. Qu, J. Luo, and J. Luo, J. Neurosci. Methods **185**, 307 (2010).
[67] M. Moscovici, W.-Y. Chien, M. Abdelgawad, and Y. Sun, Biomicrofluidics **4**, 046501 (2010).